J. Fluid Mech. (1997), *vol.* 332, *pp.* 23–39

Cross-streamline migration of slender Brownian fibres in plane Poiseuille flow

By RICHARD L. SCHIEK AND ERIC S. G. SHAQFEH
Department of Chemical Engineering, Stanford University, Stanford, CA 94305-5025, USA

(Received 3 September 1995 and in revised form 18 June 1996)

We consider fibre migration across streamlines in a suspension under plane Poiseuille flow. The flow investigated lies between two infinite, parallel plates separated by a distance comparable to the length of a suspended fibre. We consider the *weak flow limit* such that Brownian motion strongly affects the fibre position and orientation. Under these conditions, the fibre distribution, fibre mobility and fluid velocity field all vary on scales comparable to the fibre's length thus complicating a traditional volume-averaging approach to solving this problem. Therefore, we use a non-local derivation of the stress. The resulting fully coupled problem for the fluid velocity, fibre stress contribution and fibre distribution function is solved self-consistently in the limit of strong Brownian motion. When calculated in this manner, we show that at steady state the fibres' centre-of-mass distribution function shows a net migration of fibres away from the centre of the channel and towards the channel walls. The fibre migration occurs for all gap widths ($0 \leqslant \lambda \leqslant 35$) and fibre concentrations ($0 \leqslant c \leqslant 1.0$) investigated. Additionally, the fibre concentration reaches a maximum value around one fibre half-length from the channel walls. However, we find that the net fibre migration is a relatively small change over the fibre's uniform bulk distribution, and typically the centre-of-mass migration changes the uniform concentration profile by only a few percent.

1. Introduction

The subject of polymer migration across streamlines has been extensively investigated and is thoroughly reviewed by Agarwal, Dutta & Mashelkar (1994). Though experimental investigations are difficult to conduct, evidence has been presented for migration in both cylindrical Couette and Poiseuille flows. Measurements have shown that a polyacrylamide suspension under shear flow in a Couette device demonstrated a 2% to 12% increase in polymer concentration in stagnant fluid cavities near the walls (Metzner, Cohen & Rangel-Nafaile 1979). In Poiseuille flow of the same suspension, Metzner *et al.* found a 5% to 30% increase in polymer concentration in stagnant fluid cavities in the walls of their Poiseuille apparatus. Such experiments imply that polymers near a wall will migrate through it when steric constraints are relieved. In contrast to Metzner's experiments, Ausserre *et al.* (1991) reported a reduction in the concentration of xanthan near a capillary tube wall. Concentration depletion layers are related to the *slip* of a fluid near a boundary but are not indicative of net polymer migration (Schiek & Shaqfeh 1995).

To theoretically explain polymer migration in rectilinear flows Aubert & Tirrell (1982) considered a bead-and-spring dumbbell in both Couette and Poiseuille flows. They found polymer migration across streamlines only in the case of circular

Couette flow. In plane Poiseuille flow, the bead and spring dumbbells were predicted to translate with a centre of mass velocity less than the local fluid velocity, but no migration across streamlines was found. Investigating the encapsulated FENE dumbbell model in plane Poiseuille flow, Brunn & Kaloni (1985) predicted migration towards and away from the channel centre depending on parameter choices within the model. While the predicted migration effect was small, it resulted from the anisotropic mobility allowed in the encapsulated FENE model. However, because the predicted migration was very small and its direction depended on model parameters, Brunn & Kaloni (1985) decided it was insignificant.

In this work we focus on slender rigid fibres as a simple polymer model possessing an anisotropic mobility (Batchelor 1970). The slender, rigid fibres will be suspended in a Newtonian solvent held between two infinite, parallel plates. Between the plates the fluid is subject to an axial pressure gradient generating plane Poiseuille flow. We allow the fibres' centre of mass to diffuse and their orientations to change under the random force of Brownian motion. The gap confining the fibre suspension is assumed to scale on the length of a suspended fibre. Confinement to a small gap causes the velocity field, fibre concentration field and fibre mobility to change on lengths comparable to the fibres' length (Schiek & Shaqfeh 1995). In this complex non-local environment, we self-consistently calculate the velocity field, fibre stress and fibre probability density function. From the probability density function, the fibres' centre of mass distribution and segmental distribution functions are calculated and show migration of the fibres towards the channel walls.

2. Governing equations

Depicted in figure 1 is the problem geometry. Suspended in a Newtonian fluid are n identical fibres per unit volume with a full length $2l$ and a diameter $2b$. The fibres' aspect ratio is considered large and thus its inverse is small, i.e. $\epsilon \equiv b/l \ll 1$. The dimensionless fibre concentration is $c = nl^3/\ln[2/\epsilon]$. Using the vector $\boldsymbol{x}_c$ to locate a given fibre's centre of mass position and the vector $\boldsymbol{p}$ to denote its orientation, we can fully specify an axisymmetric fibre's configuration. Our interest lies in the examination of a fibre suspension confined to a narrow gap between two parallel plates. The dimensional distance between the plates, h, is non-dimensionalized by the fibre half-length, l, and denoted by λ. The coordinate system used herein specifies a fibre's configuration by a scalar position, z, and two orientation angles, θ and ϕ. The scalar quantity z denotes the distance between the lower wall and the fibre's centre-of-mass. The azimuthal angle θ is defined as the angle the fibre's orientation vector, $\boldsymbol{p}$, makes with the normal to the wall, x_3. Finally, ϕ measures the angle between the projection of the orientation vector $\boldsymbol{p}$ into the (x_1, x_2)-plane, denoted by $\boldsymbol{p}'$ in figure 1, and the x_1-axis.

Calculation of the fibre's centre-of-mass distribution, denoted by $P_{cm}(z)$, requires knowledge of the full probability density function, $P(z, \theta, \phi)$, which determines the probability of finding a fibre with a specific (z, θ, ϕ) configuration. Since our interest lies in a fibre suspension under non-equilibrium conditions, the governing equations for the probability density function will depend on the fluid velocity field. Owing to the fibres in the suspension, the fluid velocity field is affected by the stress exerted by the fibres on the fluid, or the fibre extra stress. Therefore, the governing equations for our model problem describe the fibre's probability density function, fluid velocity field and the fibre's extra stress. A detailed derivation and discussion of the governing equations was completed by Schiek & Shaqfeh (1995) and will not be repeated here. In this work

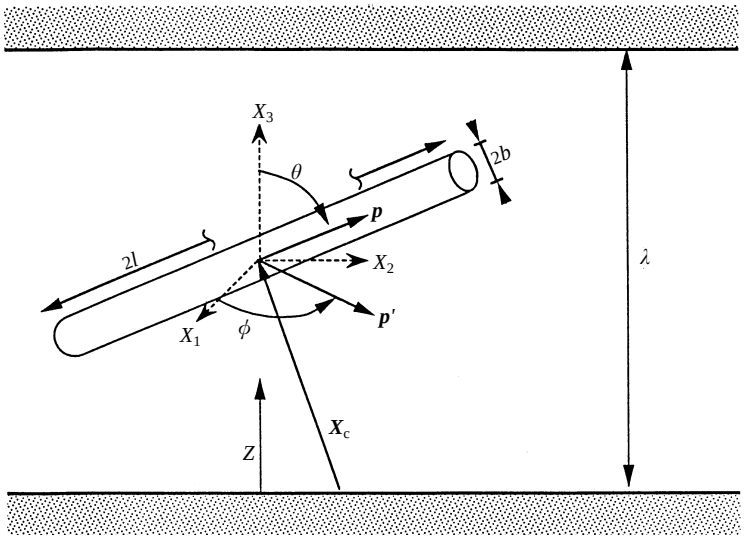

FIGURE 1. Geometry and notation used to describe a fibre suspension under flow between two infinite, parallel plates.

we will quote the governing equations from that source while briefly discussing the meaning of each equation. Thus, in the next subsection we discuss the equations governing the probability density function while in the following subsections we examine the fluid velocity and fibre stress relations.

2.1. *Fibre configuration function*: $P(z, \theta, \phi)$

To investigate the configuration of a fibre suspension subject to Brownian motion, an assumption must be made about the size of the fibres, or equivalently the relaxation time of the fibres relative to the relaxation time of the solvent. Physically, the fibres are assumed to be small enough that Brownian motion quickly changes their position and orientation, but large enough that impact of solvent molecules on the fibres can be treated as a stochastic, random force. Such an assumption is quite reasonable considering that in simple liquids it limits the fibre length to the order of microns. This is the size of many naturally occurring macromolecules, e.g. the semi-rigid Xanthan gum (Chauveteau 1982; Sorbie & Huang 1991), and the rigid molecules tropocollagen (Stryer 1988) and fibrinogen (Weisel, Phillips & Cohen 1981). The assumption that the fibres are small is equivalent to assuming that the relaxation time of the solvent is much less than the relaxation time of the fibres (Chandrasekhar 1943; McQuarrie 1976). Thus on time scales much larger than the solvent's relaxation time, a Fokker–Planck equation governs the probability density function for fibre position and orientation (Chandrasekhar 1943). A detailed derivation of the Fokker–Planck equation for this system is given in Schiek & Shaqfeh (1995) (also see Nitsche 1991 and Nitsche & Brenner 1990, but these are limited to fibre suspensions without flow). The problem geometry is shown in figure 1, where an axial pressure gradient applied in the x_2-direction produces flow with a velocity denoted by $\langle u_2 \rangle$. Under this geometry we assume that the fibre concentration is small such that $nl^3 \ll 1$. Although this strictly limits this theory to dilute fibre suspensions, the self-consistent solution method used here and in our earlier work suggests that the theory is accurate for $nl^3 \sim 1$ (Schiek & Shaqfeh 1995).

The Fokker–Planck equation for the geometry shown in figure 1 is

$$\kappa^2[1-\rho\sin^2\theta]\frac{\partial^2 P}{\partial z^2}+\frac{1}{\sin\theta}\frac{\partial}{\partial\theta}\left[\sin\theta\frac{\partial P}{\partial\theta}\right]+\frac{1}{\sin^2\theta}\frac{\partial^2 P}{\partial\phi^2}$$
$$= Pe\left\{\frac{1}{\sin\theta}\frac{\partial}{\partial\theta}[\sin\theta\cos\theta\sin\phi g(z,\theta)\,P]+\frac{1}{\sin\theta}\frac{\partial}{\partial\phi}[\cos\phi g(z,\theta)\,P]\right\}, \quad (1)$$

where the following definitions have been made:

$$g(z,\theta)=\frac{3}{2}\int_{-1}^{+1} s\langle u_2\rangle(z+s\cos\theta)\,\mathrm{d}s, \quad (2)$$

$$Pe=\dot\gamma/D_r, \quad (3)$$

$$\kappa^2=\frac{D_\parallel}{l^2 D_r}=\tfrac{2}{3} \quad \text{for slender fibres}, \quad (4)$$

$$\rho=1-\frac{D_\perp}{D_\parallel}=\tfrac{1}{2} \quad \text{for slender fibres}. \quad (5)$$

In equation (1), Pe is the Péclet number for this problem, defined as the ratio of the shear rate at the wall, $\dot\gamma$, to the fibre's rotary diffusivity, D_r.

The factor κ is a constant ratio of the fibre's parallel diffusivity, $D_\parallel$, to its rotary diffusivity, D_r, where the fibre's half-length has been used to make this ratio dimensionless. A similar constant ratio, ρ, is the ratio of the fibre's perpendicular diffusivity, $D_\perp$, to its parallel diffusivity. Both κ and ρ are easily calculated from the slender-body theory presented by Batchelor (1970). Finally, the function $g(z,\theta)$ is the average first moment of the velocity field along the fibre length. This is directly related to the fibre's rotational velocity, $\dot\theta$ and $\dot\phi$, which are given by the equations $\dot\theta=\cos\theta\sin\phi g(z,\theta)$ and $\dot\phi=\cos\phi g(z,\theta)/\sin\phi$ (Brenner 1973). All lengths have been made dimensionless with the fibre half-length l, time with $(\dot\gamma)^{-1}$ and all velocities with $\dot\gamma l$.

Originally derived for an unbound system, equation (1) does not contain information about system boundaries. Enforcing zero particle flux through the boundaries on the above Fokker–Plank equation can be achieved through the appropriate boundary conditions. A no-flux boundary condition for rigid fibres must couple translational and rotational motions, and a complete derivation is given elsewhere (Schiek & Shaqfeh 1995; Nitsche 1991; Nitsche & Brenner 1990). At present we simply quote the condition for the lower boundary as

$$-\kappa^2[1-\rho\sin^2\theta]\frac{\partial P}{\partial z}\pm\sin\theta\left(Pe\cos\theta\sin\phi g(z,\theta,\phi)\,P-\frac{\partial P}{\partial\theta}\right)=0 \quad \text{on} \quad z=\pm\cos\theta, \quad (6)$$

and on the upper boundary as

$$-\kappa^2[1-\rho\sin^2\theta]\frac{\partial P}{\partial z}\mp\sin\theta\left(Pe\cos\theta\sin\phi g(z,\theta,\phi)\,P-\frac{\partial P}{\partial\theta}\right)=0 \quad \text{on} \quad z=\lambda\mp\cos\theta. \quad (7)$$

In equations (6) and (7) the upper sign is used when $0\leqslant\theta\leqslant\frac{1}{2}\pi$ and the lower sign is used when $\frac{1}{2}\pi\leqslant\theta\leqslant\pi$ as required for proper coupling of centre-of-mass and rotational flux.

To complete the specification of the probability density function we note that the geometry dictates that $P(z,\theta,\phi)$ be periodic in ϕ as

$$P(z,\theta,\phi+2\pi)=P(z,\theta,\phi). \quad (8)$$

Finally, the probability density function must be normalized. Normalization is discussed in detail in Schiek & Shaqfeh (1995) and in the present investigation we

consider normalization subject to the constraint that the fibre suspension in the gap is in equilibrium with an unbounded suspension of the same concentration. Under this assumption, the probability density function has the form

$$P(z, \theta, \phi) = n/4\pi \tag{9}$$

within all allowed fibre configuration states and zero outside the allowed configurations when the suspension is not flowing, or $Pe = 0$ (Schiek & Shaqfeh 1995). In equation (9), n is the number of fibres per unit volume in the unbounded suspension with which the gap is in equilibrium. This normalization was determined by noting that the integral of the probability density function over all allowed centre-of-mass locations and orientations must equal the number of fibres in the suspension. Under flow, the probability density will have the prefactor, $n/(4\pi)$, multiplying a function of Pe, z, θ and ϕ whose integral over all, z, θ and ϕ is required to be unity. More explicit details on the use of this normalization will be given when solution of the governing equations is discussed in §3.

For future reference, the formula used to calculate the fibre's centre-of-mass probability density function and segmental probability density function will be presented. The centre-of-mass probability density function is derived from the full probability density function by integration over all allowed orientations, i.e. all θ and ϕ, for a given centre of mass location, z, namely

$$P_{cm}(z) = \int_{\theta_1(z)}^{\theta_2(z)} \mathrm{d}\theta \int_0^{2\pi} \mathrm{d}\phi \sin\theta P(z, \theta, \phi). \tag{10}$$

The bounds of integration for the θ-integral depend on the centre-of-mass location and are given by

$$\theta_1 = \begin{cases} 0 & \text{for} \quad z \geqslant 1 \quad \text{and} \quad z \leqslant (\lambda - 1) \\ \arccos(z) & \text{for} \quad z \leqslant 1 \\ \arccos(\lambda - z) & \text{for} \quad z \geqslant (\lambda - 1), \end{cases} \tag{11}$$

and

$$\theta_2 = \begin{cases} \pi & \text{for} \quad z \geqslant 1 \quad \text{and} \quad z \leqslant (\lambda - 1) \\ \arccos(-z) & \text{for} \quad z \leqslant 1 \\ \arccos(-\lambda + z) & \text{for} \quad z \geqslant (\lambda - 1). \end{cases} \tag{12}$$

At any point, z, in the suspension there is a finite probability of a fibre segment intersecting that point. Thus, we can also define a segmental probability density function through the expression

$$P_{sm}(z) = \int_{z_1(z)}^{z_2(z)} \mathrm{d}z_{eff} \int_{\theta_3(z_{eff})}^{\theta_4(z_{eff})} \mathrm{d}\theta \int_0^{2\pi} \mathrm{d}\phi \sin\theta P(z_{eff}, \theta, \phi), \tag{13}$$

where $z_1(z)$ and $z_2(z)$ represent the minimum and maximum centre-of-mass positions within the allowed configuration space from which fibres can intersect the point of interest z. In the bulk, $z_1(z) = z - 1$ and $z_2(z) = z + 1$ since fibres one unit length away can intersect the point of interest. Near a boundary, z_1 and z_2 are constrained to lie within the natural domain of $z \in [0, \lambda]$. The functions $\theta_3(z_{eff})$ and $\theta_4(z_{eff})$ define the minimum and maximum angles in θ that a fibre with centre of mass at z_{eff} can have and still intersect the plane of interest, z.

Because fibres change their configuration when the fluid surrounding them moves, the governing partial differential equation for the probability density function and the

no-flux boundary conditions depend on the fluid velocity. Since the fluid velocity is assumed to change on the length scale of the fibre, the probability density function depends on an integral average of the velocity through the function $g(z,\theta)$ in equation (2). In the following subsection the equations governing the fluid velocity field are summarized, as derived in our previous publication (Schiek & Shaqfeh 1995).

2.2. *Momentum conservation and fluid velocity*: $\langle u_i \rangle$

The motion of the Newtonian fluid of our fibre suspension is governed by Cauchy's equation of motion; however, the presence of the fibres adds an additional stress term and a body force term. The extra stress due to the fibres arises because the rigid fibres cannot obey the Newtonian stress relationship of the solvent. Because we have assumed that the fibres' positions and orientations and influenced by Brownian motion, the Brownian movement of the fibres imparts an additional force density on the fluid. Schiek & Shaqfeh (1995) derived the following momentum equation for a Brownian fibre suspension:

$$\mu\frac{\partial^2\langle u_j\rangle}{\partial x_i\partial x_j}+\frac{\partial\langle\sigma'_{ij}\rangle}{\partial x_j}-\frac{\partial\langle\mathscr{P}\rangle}{\partial x_i}=\int_\Omega \mathrm{d}\boldsymbol{p}\int_{-l}^{+l}\mathrm{d}s\left(\frac{1}{2l}\right)\mathscr{F}_i(\boldsymbol{x}-s\boldsymbol{p},\boldsymbol{p})\,P(\boldsymbol{x}-s\boldsymbol{p},\boldsymbol{p}), \tag{14}$$

Quantities appearing in angle brackets are ensemble averaged over all possible configurations of fibres within the suspension using the definition of an ensemble average found in McQuarrie (1976). The ensemble-averaged fluid velocity is denoted by $\langle u_j\rangle$, while the extra stress and pressure field are denoted by $\langle\sigma'_{ij}\rangle$ and $\mathscr{P}$ respectively. The constant μ represents the viscosity of the pure Newtonian solvent which is suspending the fibres. Finally, $\mathscr{F}_i$ is related to the Brownian force through a gradient of a potential, $\mathscr{U}$ (Doi & Edwards):

$$\mathscr{U}=k_B\,T\ln\left[P(\boldsymbol{x}_c,\boldsymbol{p})\right] \tag{15}$$

and

$$\mathscr{F}_i=-\frac{\partial\mathscr{U}}{\partial x_{ci}}. \tag{16}$$

In (15), k_B is Boltzmann's constant and T is the absolute temperature. To finish the discussion of the governing equations, the extra stress generated by the fibres on the fluid must be accounted for in the momentum balance of (14).

2.3. *The fibre non-local extra stress*: $\langle\sigma'_{ij}\rangle$

The non-local extra stress caused by the fibres at some point of interest, $\boldsymbol{x}$, was derived by Schiek & Shaqfeh (1995) as

$$\begin{aligned}\langle\sigma'_{ij}\rangle(\boldsymbol{x})=&\frac{2\pi\mu}{\ln(2/\epsilon)}\int_\Omega \mathrm{d}\boldsymbol{p}\int_{-2l}^{+2l}\mathrm{d}\xi\,W_1(\xi)\,p_ip_jp_kp_l\frac{\partial\langle u_k\rangle}{\partial x_l}(\boldsymbol{x}+\xi\boldsymbol{p})\\&+\frac{2\pi\mu}{\ln(2/\epsilon)}\int_\Omega \mathrm{d}\boldsymbol{p}\int_{-2l}^{+2l}\mathrm{d}\xi\,W_2(\xi)\,(\delta_{ik}-p_ip_k)p_jp_l\frac{\partial\langle u_k\rangle}{\partial x_l}(\boldsymbol{x}+\xi\boldsymbol{p})\\&-\frac{3}{2l^3}\int_\Omega \mathrm{d}\boldsymbol{p}\int_{-l}^{+l}\mathrm{d}s\left(\frac{s^2-l^2}{2}\right)P(\boldsymbol{x}-s\boldsymbol{p},\boldsymbol{p})\,\epsilon_{imn}p_jp_m\,\mathscr{N}_n(\boldsymbol{x}-s\boldsymbol{p}\,|\,\boldsymbol{p}).\end{aligned} \tag{17}$$

The domain of integration, Ω, refers to the complete set of orientations, $\boldsymbol{p}$. Exclusion of forbidden configurations (i.e. configurations that would place part of a fibre in a wall) from the extra stress occurs through the probability density function, $P(z,\theta,\phi)$.

Since the probability density function is defined as zero for unallowed configurations, any combination of centre-of-mass positions given by $\boldsymbol{x}+\xi\boldsymbol{p}$ or $\boldsymbol{x}-s\boldsymbol{p}$ and orientations, $\boldsymbol{p}$, in (17) that is not an allowed configuration has no effect on the averaging. In (17), the unit alternating tensor is denoted by ϵ_{imn}. Finally $W_1(\xi)$ and $W_2(\xi)$ in (17) are weighting functions defined as

$$W_1(\xi) = \begin{cases} \displaystyle\int_{-l}^{l-\xi} \frac{(l-s)(l-\xi-s)}{2l} P(\boldsymbol{x}-s\boldsymbol{p},\boldsymbol{p})\,\mathrm{d}s & \text{for} \quad \xi \geqslant 0 \\ \displaystyle\int_{-l-\xi}^{l} \frac{(l-s)(l+\xi+s)}{2l} P(\boldsymbol{x}-s\boldsymbol{p},\boldsymbol{p})\,\mathrm{d}s & \text{for} \quad \xi \leqslant 0 \end{cases} \tag{18}$$

and

$$W_2(\xi) = \begin{cases} \displaystyle\int_{-l}^{l-\xi} \frac{(l+s)(-l+\xi+s)(-l^2-3s^2+3l\xi-3s\xi)}{4l^3} P(\boldsymbol{x}-s\boldsymbol{p},\boldsymbol{p})\mathrm{d}s & \text{for} \quad \xi \geqslant 0 \\ \displaystyle\int_{l-\xi}^{-l} \frac{(l-s)(l+\xi+s)(l^2+3s^2+3l\xi+3s\xi)}{4l^3} P(\boldsymbol{x}-s\boldsymbol{p},\boldsymbol{p})\,\mathrm{d}s & \text{for} \quad \xi \leqslant 0. \end{cases} \tag{19}$$

In the non-local extra stress, equation (17), the first two integrals arise from purely hydrodynamic forces. The first integral represents extra stress caused by velocity gradients parallel to the fibre's major axis. In the limit of a uniform velocity gradient, uniform fibre mobility and fibre concentration, this integral simplifies to the extra stress in an unbounded suspension of slender, rigid, non-Brownian fibres (Batchelor 1970; Hinch & Leal 1972, 1975, 1976; Schiek & Shaqfeh 1995) as

$$\sigma'_{ij} = \frac{8\pi n l^3}{3\ln[2/\epsilon]}\{\langle p_i p_j p_k p_l\rangle - \tfrac{1}{3}\delta_{ij}\langle p_k p_l\rangle\}\frac{\partial u_k}{\partial x_l}. \tag{20}$$

In (20), the angle brackets denote averages over the fibres' orientation distribution function.

The second integral in the definition of the extra stress, equation (17), also arises from hydrodynamic forces, but is *purely non-local* in nature. To be specific, when the fluid velocity gradient field changes on lengths comparable to a fibre's length, a fibre cannot rotate with the fluid. Rather, the fibre will rotate with some average of the fluid's vorticity over its entire length. Thus there will be relative motion between the fibre and fluid causing an additional source of stress. The kernel of this integrand selects components of the velocity gradient field which are perpendicular to the fibre's major axis. As the fluid velocity field becomes constant over the length of a fibre, this integral vanishes.

The third term in (17) relates a general body torque, $\mathscr{N}_n$, experienced by the fibres to the fibres' extra stress contribution. Inclusion of a body torque allows inclusion of Brownian motion in the extra stress, since the torque generated by Brownian motion can be expressed as a gradient in a potential field which is proportional to the probability density function (Doi & Edwards 1989). This is accomplished through (15) and the expression

$$\mathscr{N}_i = -\epsilon_{ijk} p_j \frac{\partial \mathscr{U}}{\partial p_k}. \tag{21}$$

The equations of §§2.1, 2.2 and 2.3 completely specify the rheology of a confined, dilute fibre suspension under flow. In the next section the governing equations will be simplified and solved in the limit of strong Brownian motion, i.e. $Pe \ll 1$.

3. Solution techniques

Equations (1), (6), (7), (14) and (17) form a coupled set of integro-differential equations, whose solution is non-trivial. Since the focus of this work is suspensions dominated by Brownian motion, i.e. weak flow systems, where the Péclet number is small, it is natural to seek a solution as a power series in this small parameter. Expanding the probability density, fluid velocity and extra stress in terms of the Péclet number as

$$P = P^{(0)} + Pe\,P^{(1)} + Pe^2\,P^{(2)} + \ldots, \tag{22}$$

$$\langle u_2 \rangle = \langle u_2 \rangle^{(0)} + Pe\langle u_2 \rangle^{(1)} + Pe^2\langle u_2 \rangle^{(2)} + \ldots, \tag{23}$$

$$\langle \sigma_{ij} \rangle = \langle \sigma_{ij} \rangle^{(0)} + Pe\langle \sigma_{ij} \rangle^{(1)} + Pe^2\langle \sigma_{ij} \rangle^{(2)} + \ldots, \tag{24}$$

and substituting into the governing equations, we simplify the nonlinear products of probability and velocity in (17) by separating such products at different powers of the Péclet number.

The greatest advantage of this asymptotic expansion solution scheme is the simplification that results in solving for the probability density function. As posed in (1), the probability density function depends on the three variable coordinates, (z, θ, ϕ), as well as the flow strength as measured by the Péclet number, Pe. The asymptotic expansion method gives the form of the Péclet number dependence, for $Pe \ll 1$, while simultaneously making the governing equations separable in the variable ϕ. Substituting the expansion (22) into (1), (6) and (7) allow one to conclude by inspection that the form of the probability density function to order Pe^2 is

$$P(z, \theta, \phi) = \frac{n}{4\pi}\{1 + Pe \sin\phi \mathscr{H}(z, \theta) + Pe^2[\mathscr{G}_1(z, \theta) + \sin\phi \mathscr{G}_2(z, \theta) + \cos(2\phi)\mathscr{G}_3(z, \theta)]\}. \tag{25}$$

Without flow, when $Pe = 0$, the above expansion reduces to the equilibrium probability density function given in (9).

The boundary value problem for $\mathscr{H}(z, \theta)$ is

$$\kappa^2[1 - \rho\sin^2\theta]\frac{\partial^2\mathscr{H}}{\partial z^2} + \frac{1}{\sin\theta}\frac{\partial}{\partial\theta}\left[\sin\theta\frac{\partial\mathscr{H}}{\partial\theta}\right] - \frac{\mathscr{H}}{\sin^2\theta} = \tfrac{3}{2}\sin\theta[\langle u_2 \rangle^{(0)}(z - \cos\theta) - \langle u_2 \rangle^{(0)}(z + \cos\theta)], \tag{26}$$

subject to the boundary conditions

$$-\kappa^2[1 - \rho\sin^2\theta]\frac{\partial\mathscr{H}}{\partial z} \mp \sin\theta\frac{\partial\mathscr{H}}{\partial\theta} \pm \sin\theta\cos\theta g(z, \theta\,|\,\langle u_2 \rangle^{(0)}) = 0 \tag{27}$$

on $z = \pm\cos\theta$ and

$$-\kappa^2[1 - \rho\sin^2\theta]\frac{\partial\mathscr{H}}{\partial z} \pm \sin\theta\frac{\partial\mathscr{H}}{\partial\theta} \mp \sin\theta\cos\theta g(z, \theta\,|\,\langle u_2 \rangle^{(0)}) = 0 \tag{28}$$

on $z = \lambda \mp \cos\theta$. Similarly, the boundary value problem for $\mathscr{G}_1(z, \theta)$ is

$$\kappa^2[1 - \rho\sin^2\theta]\frac{\partial^2\mathscr{G}_1}{\partial z^2} + \frac{1}{\sin\theta}\frac{\partial}{\partial\theta}\left[\sin\theta\frac{\partial\mathscr{G}_1}{\partial\theta}\right] = \left\{\cos\theta g(z, \theta\,|\,\langle u_2 \rangle^{(0)})\frac{\partial\mathscr{H}}{\partial\theta} + \frac{1}{\sin\theta}g(z, \theta\,|\,\langle u_2 \rangle^{(0)})\mathscr{H} + \tfrac{3}{2}\sin\theta\mathscr{H}[\langle u_2 \rangle^{(0)}(z - \cos\theta) - \langle u_2 \rangle^{(0)}(z + \cos\theta)]\right\} \tag{29}$$

subject to the boundary conditions

$$-\kappa^2[1-\rho\sin^2\theta]\frac{\partial \mathscr{G}_1}{\partial z}\mp\sin\theta\frac{\partial \mathscr{G}_1}{\partial \theta}\pm\tfrac{1}{2}\sin\theta\cos\theta g(z,\theta\,|\,\langle u_2\rangle^{(0)})\,\mathscr{H}=0 \tag{30}$$

on $z=\pm\cos\theta$ and

$$-\kappa^2[1-\rho\sin^2\theta]\frac{\partial \mathscr{G}_1}{\partial z}\pm\sin\theta\frac{\partial \mathscr{G}_1}{\partial \theta}\mp\tfrac{1}{2}\sin\theta\cos\theta g(z,\theta\,|\,\langle u_2\rangle^{(0)})\,\mathscr{H}=0 \tag{31}$$

on $z=\lambda\mp\cos\theta$.

Calculation of the function $\mathscr{H}(z,\theta)$ was presented in Schiek & Shaqfeh (1995). Calculation of the centre-of-mass probability density function, equation (10), and the segmental distribution function, equation (13), only depend on the order-Pe^0 term of $P(z,\theta,\phi)$ and the term $\mathscr{G}_1$ at order Pe^2 because all other terms vanish when integrated over the ϕ-domain of $[0,2\pi]$. We proceed with the solution of the equations for $\mathscr{H}(z,\theta)$, $\mathscr{G}_1(z,\theta)$, $\langle u_2\rangle^{(0)}(z)$ and $\langle\sigma'_{23}\rangle^{(0)}(z)$ by transforming the θ-coordinate with $t=\cos\theta$ which linearizes the domain boundary of $\mathscr{H}(z)$ and $\mathscr{G}_1$ from $z=|\cos\theta|$ near the walls to $z=|t|$. On the linearized domain finite differencing of the governing equations reduces the system to a stiff set of linear equations. The linear set of governing equations was solved using singular value decomposition under several mesh refinements until the results were unchanged to at least one part in 10^3.

4. Numerical results

Following the numerical calculation of the function $\mathscr{G}_1(z,\theta)$, application of (10) allows one to calculate the fibre's centre-of-mass distribution function. Plotted in figure 2(*a*) is the centre-of-mass distribution function for a fibre suspension of concentration $c=1.00$ and a gap width of $\lambda=5.0$. The function is shown for a quiescent suspension not under flow where $Pe=0$ and for a system under flow where $Pe=10.0$. Since this function is symmetric about the gap's centre, it is plotted for only half of the channel. While the governing equations were solved assuming that $Pe\ll 1$, the solution shown in figure 2(*a*) was calculated at a much higher value of Pe for two reasons. First, for a series solution to be asymptotic, one does not require that the coefficients multiplying each order solution are small, but rather requires that the product of the coefficient and the solution at each order be small relative to the solution at the previous order (Erdélyi 1956). Referring to our proposed series solution in (22), the series is asymptotic if $P^{(0)}<Pe\,P^{(1)}$ and $Pe\,P^{(1)}<Pe^2\,P^{(2)}$ which is true for $Pe=10.0$. Secondly, because the corrections to the centre-of-mass distribution function are small, plotting them at an extreme value of Pe makes the changes more evident. Examination of figure 3 shows that under flow the fibre's centre-of-mass distribution decreases in the centre of the channel and increases near the walls. The kink in the centre-of-mass distribution at $z=1.0$ is not an artifact of the calculations. At the dimensionless distance of $z=1.0$, which corresponds to a distance of one fibre half-length, the fibres can approach the wall to a distance of $O(\epsilon)$ which as $\epsilon\to 0$ appears as a fibre–wall contact (cf. figure 3). Fibre–wall contact creates a sterically excluded region of fibre configurations near the wall such that the fibre's centre-of-mass distribution declines near the wall regardless of the fluid motion (Magda, Tirrell & Davis 1988). The sterically excluded region near the wall causes the fibre concentration to decrease and contributes to a fluid *slip layer* (Schiek & Shaqfeh 1995). As figure 3 demonstrates, the migration of fibres during flow causes a decrease in the centre of mass concentration in the centre of the channel with an increase near the wall and a maximum at one fibre half-length from the wall.

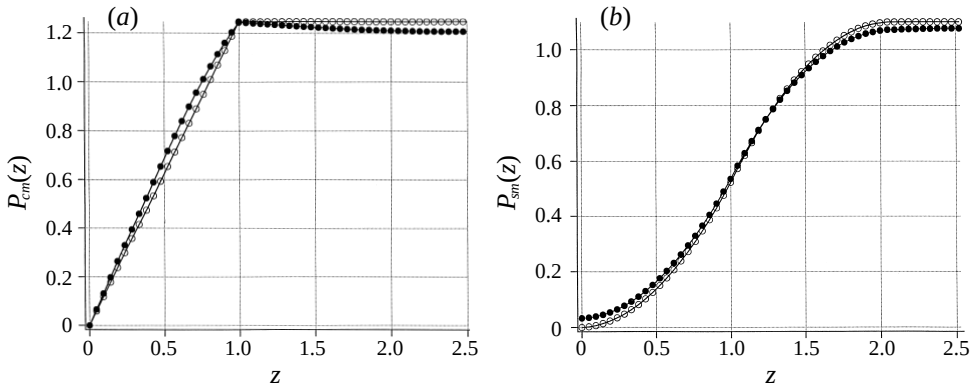

FIGURE 2. (*a*) The fibre's centre-of-mass distribution, $P_{cm}(z)$, and (*b*) the fibre's segmental distribution, $P_{sm}(z)$, to $O(Pe^2)$, for a fibre concentration of $c = 1.0$ and a gap width of $\lambda = 5.0$. The open circles denote the distribution when the fluid is stationary ($Pe = 0$) while the filled circles denote the suspension under flow with $Pe = 10.0$. Since the distribution is symmetric about the channel's centre, it is only shown up to $z = \lambda/2$.

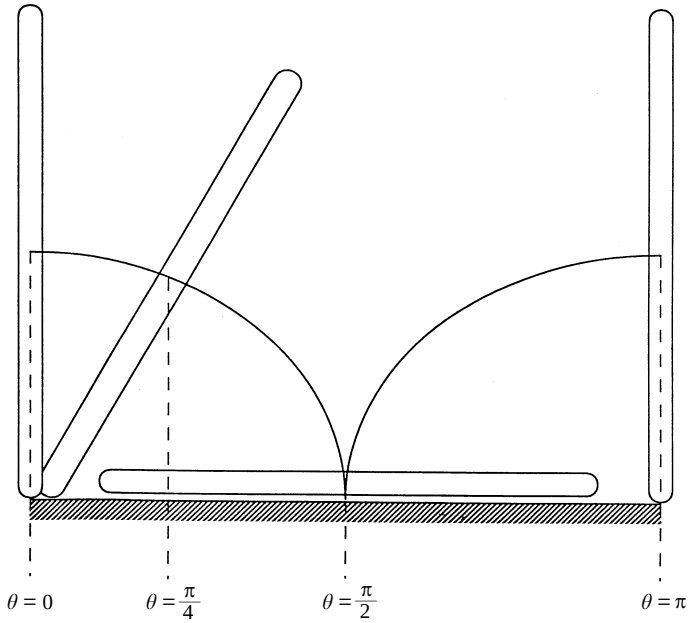

FIGURE 3. Steric constraints for a fibre in contact with a solid boundary.

Using (13), the segmental probability density function was calculated and is shown in figure 2(*b*). As with the plot of the centre-of-mass distribution, $P_{sm}(z)$ was calculated for a suspension of concentration $c = 1.0$ in a gap of width $\lambda = 5.0$ at $Pe = 0$ and 10.0. Like the centre-of-mass distribution function, the segmental distribution function

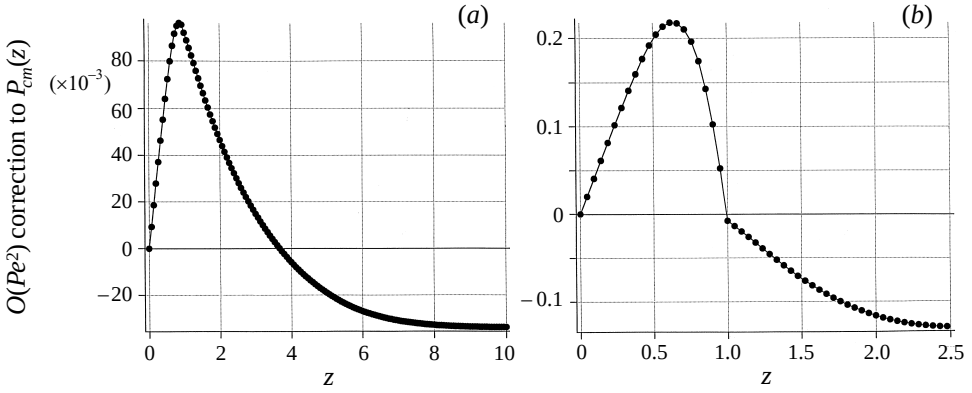

FIGURE 4. The $O(Pe^2)$ correction to the centre-of-mass probability density function for a fibre concentration of $c = 1.00$, and a gap width of (*a*) $\lambda = 20.0$ and (*b*) $\lambda = 5.0$.

shows a decrease in the fibre segment density near the centre of the channel and an increase near the walls when the suspension is under motion. Additionally, the changes in segment density are small, but this is consistent with existing experimental evidence of cross-streamline migration (Metzner *et al.* 1979).

For a clearer understanding of the origin of this cross-streamline migration we will examine the $O(Pe^2)$ correction to the centre-of-mass distribution function. Shown in figures 4(*a*) and 4(*b*) are the $O(Pe^2)$ corrections to the centre-of-mass distribution function at a fibre concentration of $c = 1.0$ and gap widths of $\lambda = 20.0$ and 5.0 respectively. To make the functions in figures 5 and 6 directly comparable, they are computed at the same volumetric flow rate, which ensures that for both figures the same number of fibres are crossing the z-plane per unit time. As can be seen in figure 4(*a*), the correction to the centre-of-mass distribution function is large and positive near the wall but decays to a shallow negative value in the channel's centre. Though slightly contracted, the correction to the centre-of-mass distribution shown in figure 4(*b*) for the narrower gap of $\lambda = 5.0$ follows the same pattern. It is large and positive near the walls and decays to a shallow negative value in the channel's centre.

The mechanism for this accumulation near the wall and depletion from the centre is readily understood. Two features are required for migration to occur. First, the suspended particle must possess an anisotropic diffusivity. Secondly, the velocity field must vary to produce a position-dependent mean orientation. For a suspension of slender, rigid fibres, the elongated bodies possess different diffusivities or drag coefficients for motion parallel and perpendicular to their central axis. For slender bodies, the parallel diffusivity is greater than the perpendicular diffusivity by approximately a factor of 2 (Batchelor 1970). Additionally, a fibre's rotational diffusivity is larger than the ratio of the translational diffusivity and l^2, as seen in (4), allowing Brownian motion to alter a fibre's orientation more rapidly than its centre of mass position. Inspection of (1) and (4) shows that $\kappa^2 \gg 0$ is required for fibre migration to occur. An anisotropic diffusivity which leads to a faster rotational diffusion time scale relative to the translational diffusion time scale fulfils the first requirement for migration (Nitsche & Hinch 1997). Near the channel edges, for all fibre concentrations, the plane Poiseuille flow velocity profile is near that of a linear shear flow (Schiek & Shaqfeh 1995) and thus the fibre's most likely orientation is parallel to the flow (and the walls). In the channel centre, the flow is plug-like at high concentrations and even at low concentrations the shear rates are small (Schiek &

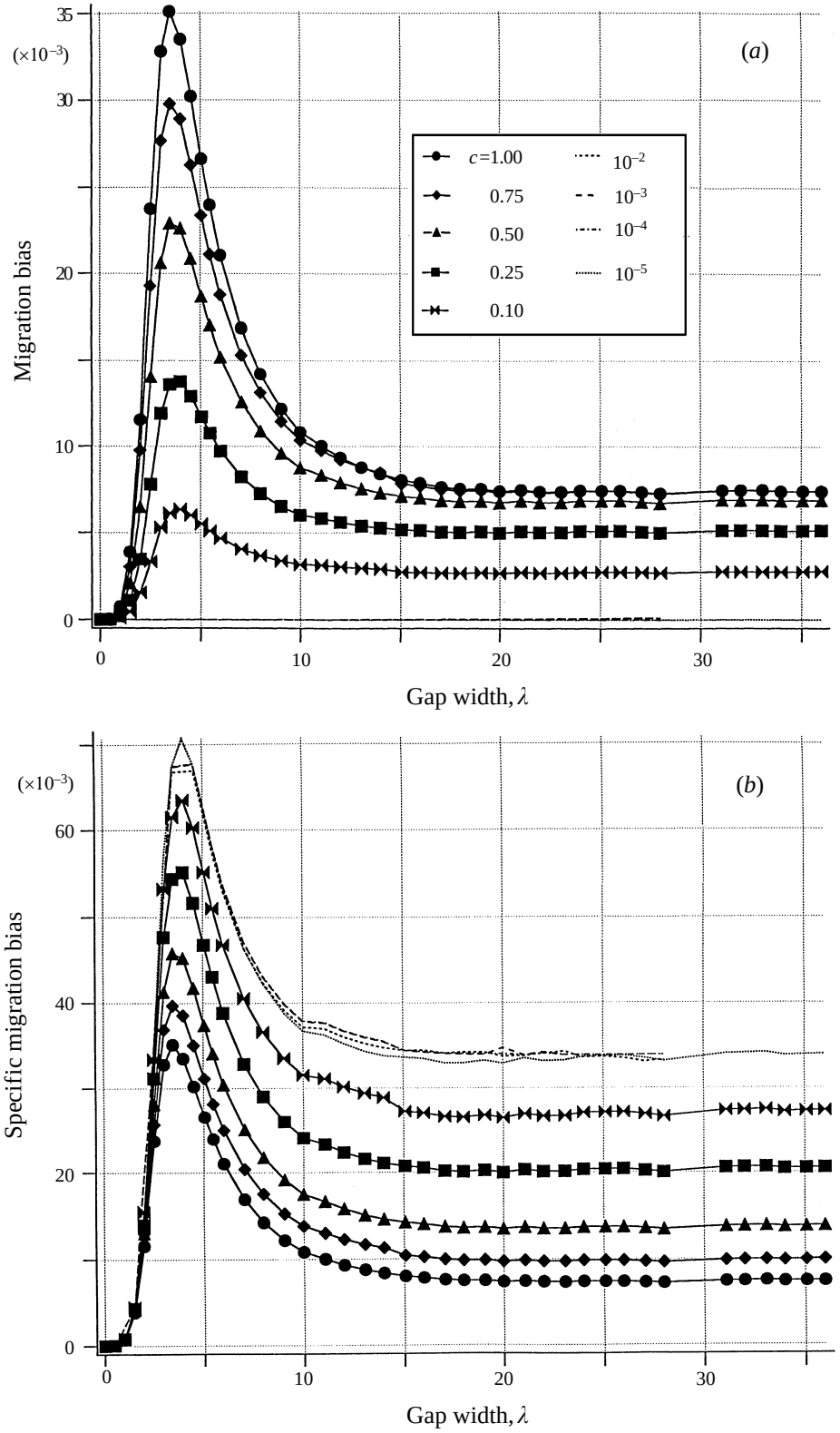

FIGURE 5. (*a*) The *migration bias* as a function of gap width and fibre concentration. (*b*) The *migration bias* per concentration as a function of gap width and concentration.

Shaqfeh 1995). Owing to Brownian motion and the very low shear rate near the channel centre, fibres there will have a nearly random orientation distribution. Hence, the nonlinear velocity profile causes a position-dependent mean fibre orientation meeting the second requirement for migration. Considering diffusive motion perpendicular to the bounding walls, the fibres near the walls will on average have a lower diffusivity than the fibres in the channel centre since their most probable orientation is parallel to the flow. Thus, fibres that diffuse from the centre of the channel towards a wall encounter a velocity field that changes their mean orientation to a configuration with a lower diffusivity perpendicular to the walls. Since the translational and rotational diffusion time scales are different, translational diffusion back to the centre of the channel cannot occur before a fibre can change its orientation. Fibres that have migrated towards the walls acquire a lower diffusivity for motion perpendicular to the walls and thus require more time to migrate back towards the centre of the channel. Thus, fibres will accumulate near the walls (Nitsche & Hinch 1997).

Another measure of the tendency for fibres to migrate is the total positive area beneath the $O(Pe^2)$ correction to the centre-of-mass distribution function. The magnitude of this positive area is a direct measure of the probability for fibre migration and we will refer to this area as the *migration bias*. In figure 5(*a*) the migration bias is plotted as a function of total gap width and concentration. All the results in this graph were calculated at a constant volumetric flow rate for the suspension, allowing direct comparison between points at different concentrations and gap widths. The migration bias is strongly dependent on gap width for small gaps, reaching a maximum around $\lambda = 4$. For large gap widths, the migration bias approaches a constant value. Although we have assumed that the suspension is dilute, the migration bias is not a linear function of concentration. The nonlinear concentration dependence of the migration bias is best demonstrated by the results for $c = 1.00$ and 0.75 in figure 5(*a*). If the migration bias were linear in concentration then the lines for $c = 1.00$ and 0.75 would not cross; however at large gap widths the lines intersect.

To further investigate the concentration dependence of the migration bias, we can consider the ratio of the migration bias to the concentration. This *migration bias per unit concentration* or specific migration bias is plotted in figure 5(*b*) and it is a measure of the strength or driving force behind migration. From figure 5(*b*), it can be seen that the specific migration bias follows the same general trend as the migration bias, being largest for gaps near $\lambda = 4$ and constant at large gaps. It is important to note that the specific migration bias is greatest for the lowest concentrations investigated. Thus, the driving force behind migration is strongest for dilute suspensions. However, concentrated suspensions show a stronger migration bias as shown in figure 5(*a*) despite having the weaker driving potential as seen in figure 5(*b*). Within our theory, the primary effect of increasing the fibre concentration on the probability density function is to change the mean velocity field. Dilute suspensions thus perturb the velocity profile from its Newtonian form only slightly compared to concentrated suspensions. In a Newtonian parabolic velocity field, once a fibre diffuses off the centreline, it immediately has a lower effective diffusivity since the weak shear rate aligns the fibre with the flow thus reducing its diffusivity. In a more concentrated suspension where the velocity profile is *plug like* (Schiek & Shaqfeh 1995), diffusion off the centreline of the channel alters a fibre's effective diffusivity to a smaller degree because the local shear rate is lower than in the dilute suspension, and thus the effective diffusivity will remain somewhat higher.

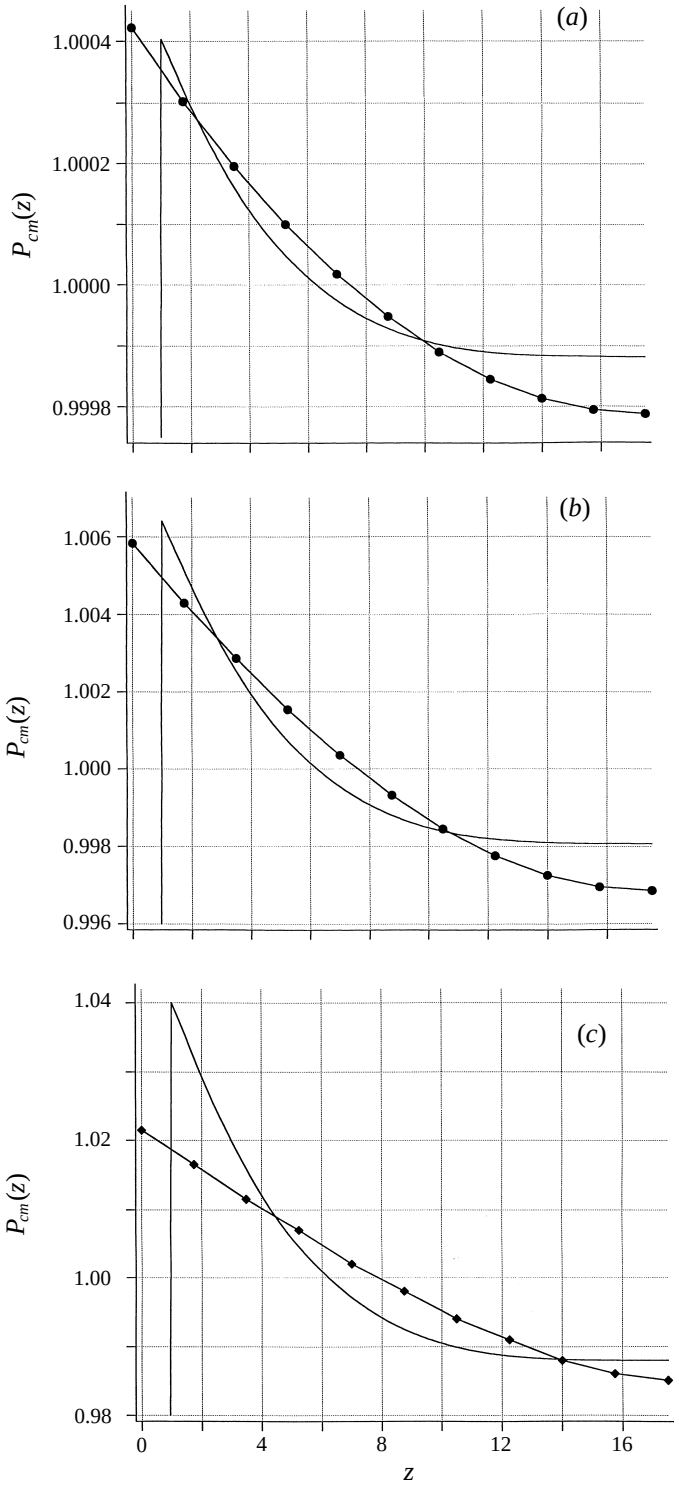

FIGURE 6. Predicted fibre centre-of-mass distributions from the non-local theory of this work for an infinitely dilute suspension, $c = 0$, confined to a gap of width $\lambda = 35.0$ (——) and the local analysis of Nitsche & Hinch (1997) (—●—). Both centre-of-mass distributions assume (*a*) $Pe = 0.5$, (*b*) $Pe = 2.0$, (*c*) $Pe = 5.0$.

5. Comparison to local analyses

Recent work by Nitsche & Hinch (1997) examines the cross-streamline migration of a dilute fibre suspension in plane Poiseuille flow. While our work examines rigorously confined fibre suspensions under strong Brownian motion, or weak flow, the study by Nitsche & Hinch focuses on fibres in a strong parabolic channel flow where Pe is $O(1)$. In order to calculate the centre-of-mass probability density function for $Pe \sim O(1)$, Nitsche & Hinch (1997) simplify the no-flux constraints of equations (6) and (7) by ignoring the orientation dependence and assuming a zero fibre centre-of-mass flux at the channel walls. Additionally, they assume that the concentration of fibres within the suspension is sufficiently dilute such that the fully developed velocity profile of the suspension is parabolic. A reasonable comparison can be made between our results and those of Nitsche & Hinch provided we make the following assumptions. First, to account for the simplified boundary conditions used by Nitsche & Hinch, we must assume that the channel width is large with respect to the depletion layers near the walls. Secondly, we must assume that the suspension concentration is small so that the resultant fluid velocity profile is parabolic. Computational resources limited the largest gap width that we considered to $\lambda = 35.0$, and in order to achieve sufficient diluteness, calculations were performed with the concentration parameter set to zero. With $c = 0$, it is necessary to factor the concentration out of the probability density, allowing it to be non-zero. Finally, Nitsche & Hinch (1997) provided their results at $Pe = 0.5$, 1.0, 2.0, 5.0 and 10.0. Since our theory was derived by assuming a small Pe, we compare our results at $Pe = 0.5$, 2.0 and 5.0, with $\lambda = 35.0$ and $c = 0$ to theirs at the same Pe in figure 6. In figure 6(a) where $Pe = 0.5$, both Nitsche & Hinch's (1997) and our results predict depletion from the centre of the channel and accumulation near the walls. However, the net migration predicted is small for such a weak flow, amounting to only 40 parts per million near the wall. In figure 6(b) the centre-of-mass distribution functions are plotted for $Pe = 2.0$. Although this Pe is $O(1)$, our results compare very well with those of Nitsche & Hinch (1997). Again, migration is predicted towards the walls with a net relative change in the concentration profile of about 0.5%. At $Pe = 5.0$, our weak flow theory over-predicts the centre-of-mass distribution as is shown in figure 6(c). While our weak flow theory predicts a 2% change in the fibre distribution function, Nitsche & Hinch predict only a 1% change. Over-prediction of the net migration by the weak flow theory is expected in the light of Nitsche & Hinch's (1997) results where they show that, above $Pe \approx 3$, migratory drift reaches a maximum and then decreases as a function of Pe (cf. figure 6 in Nitsche & Hinch 1997). Regardless of the assumptions and limitations, both our results and those of Nitsche & Hinch demonstrate that an axisymmetric particle with an anisotropic diffusivity in pressure-driven channel flow will migrate away from the centre of a channel and towards the walls.

6. Conclusions

The primary motivation for this work was to demonstrate a mechanism for fibre migration in systems with nonlinear velocity fields. We have shown that because of the anisotropy of the diffusivity fibres will migrate out of regions of low shear to regions of high shear. Though the small gap width dictated a non-local approach to our model problem, this mechanism for migration is quite general, applying to any body having an anisotropic diffusivity in a nonlinear velocity field. Although calculated corrections to the centre-of-mass probability density function are small, they qualitatively show the

experimentally verified migration of polymers towards the walls of the channel (Metzner *et al*. 1979). While this work's primary limitation is the restriction to weak flows where $Pe \ll 1$, such a restriction allows us to rigorously include steric wall effects. Imposition of the no-flux condition at the channel walls showed that the migration bias depends strongly on gap width for small gaps and reaches a constant value at large gaps. Our work also suggests that finite-Pe calculations for gap widths $0 < \lambda < 20$ may prove important in understanding fibre migration under complex flow conditions.

E.S.G.S. would like to thank the National Science Foundation for support under CPIMA Co-operative Agreement DMR-9400354-2, and the David and Lucile Packard foundation for funding through their fellowship program. Additionally, the authors would like to thank Dr E.J. Hinch for suggesting we examine fibre migration in highly confined channels.

REFERENCES

Aubert, J. H. & Tirrell, M. 1982 Effective viscosity of dilute polymer solutions near confining boundaries. *J. Chem. Phys.* **77**, 553–561.

Agarwal, U. S., Dutta, A. & Mashelkar, R. A. 1994 Migration of macromolecules under flow: the physical origin and engineering implications. *Chem. Engng Sci.* **49**, 1693–1717.

Ausserre, D., Edwards, J., Lecourtier, J., Hervet, H. & Rondelex, F. 1991 Hydro-dynamic thickening of depletion layers in colloidal solutions. *Europhys. Lett.* **14**, 33–38.

Batchelor, G. K. 1970 Slender-body theory for particles of arbitrary cross-section in Stokes flow. *J. Fluid Mech.* **44**, 419–440.

Brenner, H. 1973 Rheology of a dilute suspension of axisymmetric Brownian particles. *Intl J. Multiphase Flow* **1**, 195–341.

Brunn, P. O. & Kaloni, P. N. 1985 Concentrated polymer solutions: nonuniform concentration profiles in tube flow. *J. Chem. Phys.* **83**, 2497–2503.

Chandrasekhar, S. 1943 Stochastic problms in physics and astronomy. *Rev. Mod. Phys.* **15**, 1–89.

Chauveteau, G. 1982 Rodlike polymer solution flow through fine pores: influence of por size on rheological behavior. *J. Rheol.* **26**, 111–142.

Doi, M. & Edwards, S. F. 1989 *The Theory of Polymer Dynamics*. Oxford Science Publications.

Erdélyi, A. 1956 *Asymptotic Expansions*. Dover.

Hinch, E. J. & Leal, L. G. 1992 The effect of Brownian motion on the rheological properties of a suspension of non-spherical particles. *J. Fluid Mech.* **52**, 683–712.

Hinch, E. J. & Leal, L. G. 1975 Constitutive equations in suspension mechanics. Part 1. General formulation. *J. Fluid Mech.* **71**, 418–495.

Hinch, E. J. & Leal, L. G. 1976 Constitutive equations in suspension mechanics. Part 2. Approximate forms for a suspension of rigid particles affected by Brownian rotations. *J. Fluid Mech.* **76**, 187–208.

Magda, J. J., Tirrell, M. & Davis, H. 1988 The transport properties of rod-like particles. II. Narrow slit pores. *J. Chem. Phys.* **88**, 1207–1213.

McQuarrie, D. A. 1976 *Statistical Mechanics*. Harper Collins.

Metzner, A. B., Cohen, Y. & Rangel-Nafaile, C. 1979 Inhomogeneous flows of non-Newtonian fluids: generation of spatial concentrations gradients. *J. Non-Newtonian Fluid Mech.* **5**, 449–462.

Nitsche, J. M. 1991 Hydrodynamic coupling and non-equilibrium distribution in pore diffusion of nonspherical fine particles. *Particulate Sci. Tech.* **9**, 135–148.

Nitsche, J. M. & Brenner, H. 1990 On the formulation of boundary conditions for rigid nonspherical Brownian particles near solid walls: applications to orientation-specific reactions with immobilized enzymes. *J. Colloid Interface Sci.* **138**, 21–41.

Nitsche, L. C. & Hinch, E. J. 1997 Shear-induced lateral migration of Brownian rigid rods in parabolic channel flow. *J. Fluid Mech.* **332**, 1–21.

Schiek, R. L. & Shaqfeh, E. S. G. 1995 A nonlocal theory for stress in bound, Brownian suspensions of slender, rigid fibers. *J. Fluid Mech.* **296**, 271–324.

Sorbie, K. S. & Huang, Y. 1991 Rheological and transport effects in the flow of low-concentration Xanthan solution through porous media. *J. Colloidal Interface Sci.* **145**, no. 1, 74–89.

Stryer, L. 1988 *Biochemistry*. W. H. Freeman.

Weisel, J. W., Phillips Jr, G. N. & Cohen, C. 1981 A model from electron microscopy for the molecular structure of fibrinogen and fibrin. *Nature* **289**, 263–267.